STEM CELLS TRANSLATIONAL MEDICINE®

PLURIPOTENT STEM CELLS

Differentiation and Characterization of Dopaminergic Neurons From Baboon Induced Pluripotent Stem Cells

DOUGLAS A. GROW,[a,b,c] DENARD V. SIMMONS,[a,c] JORGE A. GOMEZ,[a,c] MATTHEW J. WANAT,[a,c] JOHN R. MCCARREY,[a,b] CARLOS A. PALADINI,[a,c] CHRISTOPHER S. NAVARA[a,b]

Key Words. Baboon • Induced pluripotent stem cells • Parkinson's disease • Neural differentiation • Dopaminergic neurons

[a]Department of Biology, University of Texas at San Antonio, San Antonio, Texas, USA; [b]San Antonio Cellular Therapeutics Institute, San Antonio, Texas, USA; [c]University of Texas at San Antonio Neurosciences Institute, San Antonio, Texas, USA

Correspondence: Christopher S. Navara, Ph.D., University of Texas at San Antonio, One UTSA Circle, San Antonio, Texas 78249, USA. Telephone: 210-458-6497; E-Mail: Christopher.navara@utsa.edu

Received April 13, 2015; accepted for publication March 23, 2016; published Online First on June 24, 2016.

1066-5099/2016/$20.00/0

http://dx.doi.org/10.5966/sctm.2015-0073

ABSTRACT

The progressive death of dopamine producing neurons in the substantia nigra pars compacta is the principal cause of symptoms of Parkinson's disease (PD). Stem cells have potential therapeutic use in replacing these cells and restoring function. To facilitate development of this approach, we sought to establish a preclinical model based on a large nonhuman primate for testing the efficacy and safety of stem cell-based transplantation. To this end, we differentiated baboon fibroblast-derived induced pluripotent stem cells (biPSCs) into dopaminergic neurons with the application of specific morphogens and growth factors. We confirmed that biPSC-derived dopaminergic neurons resemble those found in the human midbrain based on cell type-specific expression of dopamine markers TH and GIRK2. Using the reverse transcriptase quantitative polymerase chain reaction, we also showed that biPSC-derived dopaminergic neurons express *PAX6, FOXA2*, *LMX1A, NURR1,* and *TH* genes characteristic of this cell type in vivo. We used perforated patch-clamp electrophysiology to demonstrate that biPSC-derived dopaminergic neurons fired spontaneous rhythmic action potentials and high-frequency action potentials with spike frequency adaption upon injection of depolarizing current. Finally, we showed that biPSC-derived neurons released catecholamines in response to electrical stimulation. These results demonstrate the utility of the baboon model for testing and optimizing the efficacy and safety of stem cell-based therapeutic approaches for the treatment of PD. STEM CELLS TRANSLATIONAL MEDICINE *2016;5:1133–1144*

SIGNIFICANCE

Functional dopamine neurons were produced from baboon induced pluripotent stem cells, and their properties were compared to baboon midbrain cells in vivo. The baboon has advantages as a clinically relevant model in which to optimize the efficacy and safety of stem cell-based therapies for neurodegenerative diseases, such as Parkinson's disease. Baboons possess crucial neuroanatomical and immunological similarities to humans, and baboon pluripotent stem cells can be differentiated into functional neurons that mimic those in the human brain, thus laying the foundation for the utility of the baboon model for evaluating stem cell therapies.

INTRODUCTION

Parkinson's disease (PD) is a neurodegenerative disorder defined by the selective loss of dopamine (DA)-producing neurons in the substantia nigra pars compacta (SNc) [1]. The death of this cell population results in severely debilitating movement disorders, including bradykinesia, tremor, rigidity, and postural instability [2]. Cell-based replacement therapy holds potential as a long-term treatment for this disease; studies using cell replacement therapy have demonstrated amelioration of parkinsonism in rodent models of PD [3–5]. However, double-blind clinical trials in the early 2000s failed to achieve a significant therapeutic benefit, and some graft recipients experienced adverse side effects, such as graft-induced dyskinesias [6, 7]. Thus, although cell therapies have potential to treat PD, effective protocols remain lacking [8].

The variable outcomes of these previous efforts to apply cell-based approaches to humans for the treatment of PD symptoms may reflect several limitations. First, rather than enriching the graft tissue for DA cells by cell sorting or by directed differentiation, past protocols used heterogeneous populations of cells isolated from aborted human fetuses. Not only is this a controversial and scarce tissue source [9], these grafts contained unwanted cell types, including serotonergic neurons, which are believed to be the source of the observed graft-induced dyskinesias

[10–12]. A second possible explanation for graft failure is that heterologous cells increase the risk for immune rejection [12]. A third potential explanation is that the grafted cells were placed heterotopically in the striatum. The location of the graft is critical in that if the cells are not placed within the correct neurophysiological environment, they will not receive the proper inputs from other parts of the brain, thus creating potential for behavioral deficits.

Induced pluripotent stem cells (iPSCs) can be used in "patient-specific" cell-based therapies, which may mitigate the risk for graft rejection [13, 14] and circumvent the ethical hindrances that may accompany the use of fetal tissues [15]. Protocols have been developed to produce dopaminergic neurons from human embryonic stem cells and iPSCs [16]. However, studies examining cell injection sites, requisite numbers of injected cells, long-term survival of transplanted cells, appropriate cell type-specific gene expression in the transplanted cells, amelioration of nonmotor symptoms associated with PD, and avoidance of negative off-target effects (such as tumorigenicity), need to be performed in a relevant preclinical model. As a result, there is a substantial effort to develop nonhuman primate models of neurodegenerative disease and cell transplantation therapy [17–20], including animal models such as vervet monkeys [21] and rhesus macaques [22].

The olive baboon, *Papio anubis,* shares pertinent neuroanatomical commonalities with humans, including physical separation of the nuclei of the striatum [23], which is the target of dopamine neuron projections. The baboon also possesses a large gyrencephalic brain [24], a similar ratio of white matter to gray matter [25], and similar cerebral microvasculature [26–28] as those observed in the human brain. Additionally, longevity and development of nonmotor parkinsonian symptoms, including age-related loss of dopamine compensation in the baboon brain, provide a clinically relevant context in which to test the long-term safety and efficacy of cell-based therapies for treatment of PD [27, 29–31]. Finally, and of critical importance to transplantation studies, the baboon immune system more faithfully phenocopies the human immune system than do the rhesus or mouse immune systems [32–35] and therefore represents a model of choice in which to test the extent of any immunogenicity of transplanted cells [36], as well as the efficacy and safety of cell-based therapies to mitigate PD.

We recently reported the production of iPSCs from baboon fibroblasts [37]. Here we report the characterization of neurons generated from these biPSCs. We performed directed differentiation of biPSCs using developmentally relevant morphogens and growth factors to produce biPSC-derived dopaminergic neurons, and validated the specific identity and functionality of these neurons by confirming expression of dopaminergic markers and the upregulation of cell-type specific transcripts. Finally, we demonstrated that biPSC-derived neurons fired spontaneous rhythmic action potentials, that these neurons displayed stimulation-induced high-frequency action potential firing detectable by perforated patch-clamp electrophysiology, and that stimulation-evoked catecholamine release can be measured by fast-scan cyclic voltammetry. These results demonstrate the potential to derive functional dopaminergic neurons from baboon pluripotent stem cells and validate the utility of the baboon model for developing, testing, and optimizing clinically relevant cell-based therapeutic approaches to the treatment of PD.

Materials and Methods

Cell Culture

Culture of baboon iPSCs was performed as previously described [37–39]. Briefly, mitotically inactivated mouse embryonic feeders (MEFs) were seeded onto gelatin-coated tissue culture plates at a density of 2.6×10^4 cells per cm^2 in MEF medium (DMEM, 10% fetal bovine serum, 1 mM GlutaMax, 0.1 mM nonessential amino acids, 100 U/ml penicillin, 100 μg/ml streptomycin [all from Thermo Fisher Scientific Life Sciences, Waltham, MA, http://www.thermofisher.comd]). Two days after seeding, the medium was replaced with iPSC media (MEF conditioned for 48 hours, 80% knockout DMEM, 20% knockout serum replacer, 1 mM GlutaMax, 0.1 mM nonessential amino acids, 100 U/ml penicillin, 100 μg/ml streptomycin, and 4 ng/ml fibroblast growth factor [FGF-2]). biPSCs were seeded onto the MEFs, and colonies were manually passaged once every 8–10 days using a fire-polished glass Pasteur pipette. Media were replaced every 48 hours and cells were maintained at 37°C/5% CO_2.

Neural Induction

Neural differentiation was accomplished using a modified dual SMAD inhibition protocol [40, 41] (Fig. 1A). On day 0, cells were switched to DMEM/F12 medium containing 10 μM SB431542 (Sigma-Aldrich, St. Louis, MO, http://www.sigmaaldrich.com), 5 μM dorsomorphin (Sigma-Aldrich) (or 200 nM LDN193189, an analog of dorsomorphin [Stemgent, Cambridge, MA, https://www.stemgent.com/]), 10% knockout serum replacer, 2 mM GlutaMax, 100 U/ml penicillin, 100 μg/ml streptomycin, and 10 ng/ml FGF2 in DMEM/F12 (all from Thermo Fisher Scientific Life Sciences). On day 2, the medium was supplemented with 100 ng/ml FGF8 (R&D Systems, Minneapolis, MN, https://www.rndsystems.com), 2 μg/ml purmorphamine (Stemgent), and 200 ng/ml sonic hedgehog (SHh) (Peprotech, Rocky Hill, NJ, https://www.peprotech.com) (or 1 μM of smoothened agonist [SAG], an agonist of the SHh pathway [EMD Millipore, Billerica, MA, http://www.emdmillipore.com/]). There was no difference with use of dorsomorphin and SHh compared with their molecular analogs LDN193189 and SAG, respectively. Three micromoles of CHIR99021 (Stemgent) was added on day 3, and 20 ng/ml brain-derived neurotrophic factor (BDNF; Peprotech) was added beginning on day 4. SB431542 was removed after 5 days; SHh, FGF8, and purmorphamine were removed after 7 days; dorsomorphin was removed at 11 days; and CHIR99021 was removed at day 13. On day 15, rosettes were passaged onto poly-L-ornithine-coated (15 μg/ml; Sigma-Aldrich) and laminin-coated (5 μg/ml; Sigma-Aldrich) glass coverslips (Electron Microscopy Sciences, Hatfield, PA, https://www.emsdiasum.com). Neurons were then matured for 2 weeks in DMEM/F12 containing 1% N2 supplement and 2% B27 supplement (Thermo Fisher Scientific Life Sciences), 10 ng/ml BDNF (Peprotech), 20 ng/ml of glial cell-derived neurotrophic factor (GDNF; Peprotech), 0.5 mM dibutyryl cyclic adenosine monophosphate (cAMP; Sigma-Aldrich), 0.2 mM ascorbic acid (Sigma-Aldrich), 2 mM GlutaMax, 100 U/ml penicillin, and 100 μg/ml streptomycin.

Immunocytochemistry

Cells were grown on coverslips (Electron Microscopy Sciences) coated with 15 μg/ml poly-L-ornithine and 5 μg/ml laminin. At the indicated times, the medium was aspirated and the coverslips were washed with phosphate-buffered saline (PBS) composed of

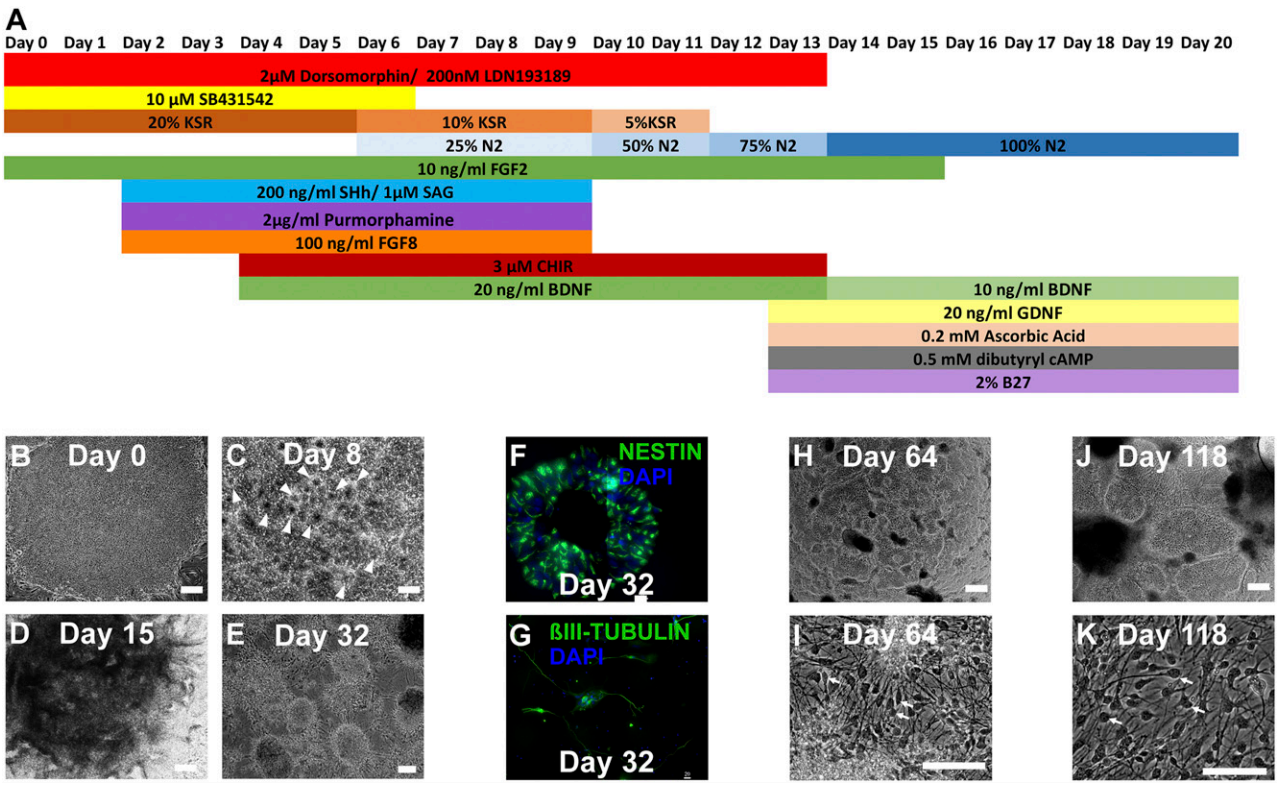

Figure 1. Progression of baboon fibroblast-derived induced pluripotent stem cells (biPSCs) to fully differentiated neurons. **(A):** Summary graph of the differentiation process. **(B):** Colony of baboon induced pluripotent stem cells before differentiation. **(C):** Colony of biPSCs after 8 days of differentiation with neural rosettes (arrowheads). **(D):** Colony of biPSCs after 15 days of differentiation just before passaging. Neural rosettes have expanded and the colony was fully confluent. **(E):** Neural precursor cells after passage. **(F):** At day 32, cells expressed early neuronal marker NESTIN. **(G):** At day 32, few cells expressed mature neuronal marker βIII-TUBULIN. **(H, J):** As the cells differentiate, they adopt a morphology with larger soma and increased branching and length of neuronal processes. This is shown in higher-magnification images **(I)** and **(K)** (arrows). All scale bars = 100 μm. Abbreviations: BDNF, brain-derived neurotrophic factor; DAPI, 4′,6-diamidino-2-phenylindole; FGF8, fibroblast growth factor 8; GDNF, glial cell-derived neurotrophic factor; KSR, knockout serum replacer; SAG, smoothened agonist; SHh, sonic hedgehog.

136.94 mM NaCl, 9.74 mM sodium phosphate dibasic, 1.70 mM potassium phosphate monobasic, and 2.65 mM KCl in 18 MΩ H_2O (PBS). The coverslips were then placed into 2% paraformaldehyde for 30 minutes at 37°C and washed three times in PBS with 0.5% Triton-X-100 (PBS-TX-100). Cell membranes were permeabilized by incubation in PBS-TX-100 for 15 minutes at room temperature and then blocked for 1 hour using 0.3% bovine serum albumin and 5% goat or donkey serum in PBS-TX-100 at room temperature. Primary antibodies were applied overnight at 4°C. Antibodies and their concentrations are listed in supplemental online Table 1. After washing three times with PBS-TX-100, coverslips were incubated in an appropriate fluorescently labeled secondary antibody (1:300) for 1 hour at room temperature. Coverslips were then washed and mounted onto microscope slides, coated with ProLong Gold Antifade with 4′,6-diamidino-2-phenylindole (DAPI; Thermo Fisher Scientific Life Sciences), covered with a cover glass, and allowed to cure for 24 hours at room temperature before imaging.

Imaging was performed using a Deltavision Personal DV system equipped with high-numerical-aperture objectives and a CoolSnap HQ2 cooled CCD camera (Applied Precision, Issaquah, WA, http://www.photometrics.com). Images were prepared for publication using SoftWorx (Applied Precision), ImageJ [42], and Photoshop (Adobe Systems, New York, Nym http://www.adobe.com/) software. Cell counts were obtained by capturing at least nine random fields of view at magnification of $\times$60. DAPI-positive cells within captured images were then counted manually using ImageJ software [42].

Immunohistochemistry of the Baboon Midbrain

The Institutional Animal Care and Use Committee of the Texas Biomedical Research Institute/Southwest National Primate Research Center in San Antonio approved all baboon experiments. Brains were removed at necropsy from baboons that were euthanized for other research purposes. The midbrain was sectioned into 0.4-cm sections using a custom baboon brain matrix and immersed in 4% ice-cold paraformaldehyde for 2 hours at 4°C. After 2 hours, the midbrain sections were washed and incubated in fresh 4% paraformaldehyde overnight at 4°C. Midbrain sections were then incubated in 30% sucrose at 4°C until they sank (approximately 48 hours). They were then washed with PBS and embedded in optimal cutting temperature medium. Sections of midbrain were cryosectioned to yield 60-μm slices that were then incubated in ice-cold PBS as floating sections, transferred to ice-cold PBS-TX-100 for 15 minutes, blocked with 10% normal goat or donkey serum in PBS-TX-100 for 1 hour at room temperature, and incubated in the indicated primary antibody (1:500) overnight at 4°C. Floating sections were then washed and incubated in the appropriate secondary antibody (1:500) for 1 hour at room temperature, washed,

and mounted to glass microscope slides with ProLong Gold Antifade with DAPI and covered with a coverglass. The mounting medium was allowed to cure for 24 hours before imaging. Baboon midbrain anatomy was identified as previously described [43].

For diaminobenzidine (DAB) staining, we used the second-generation Histostain-*Plus* kit (Thermo Fisher Scientific Life Sciences) according to the manufacturer's instructions. Sections were incubated in primary antibody as described earlier in the text, then washed and incubated in peroxidase suppressor (Thermo Fisher Scientific Life Sciences) for 15 minutes at room temperature to block endogenous peroxidase activity. Sections were then washed three times and incubated in the appropriate biotinylated secondary antibody (all from Thermo Fisher Scientific Life Sciences) for 10 minutes at room temperature. They were washed three times again before incubation in horseradish peroxidase (HRP) conjugate for 10 minutes at room temperature. Sections were washed again three times and then developed using a solution of DAB chromogen and hydrogen peroxide for 15 minutes at room temperature. Finally, sections were washed five times with ultrapure water (Thermo Fisher Scientific Life Sciences) before mounting in 50% glycerol in PBS. Baboon sections that had undergone DAB staining were imaged using a Nikon SMZ1500 stereoscope equipped with a Nikon DS-Fi1 camera and NIS Elements software (Nikon, Tokyo, Japan, http://www.nikon.com/).

RNA Isolation and cDNA Synthesis

Cells were lysed and RNA was isolated using TRIzol reagent (Thermo Fisher Scientific Life Sciences) followed by chloroform-mediated phase separation. RNA was precipitated using 100% isopropanol and washed with 75% ethanol. All RNA isolates were treated with an Ambion RNA clean-up kit with DNase to remove any genomic DNA contaminant (Thermo Fisher Scientific Life Sciences). RNA was inspected for purity and concentration using a NanoDrop spectrophotometer (Thermo Fisher Scientific Life Sciences). One microgram of the RNA isolate was converted to cDNA using the SuperScript III First Strand cDNA Synthesis kit (Thermo Fisher Scientific Life Sciences). For each sample, one additional cDNA synthesis reaction was prepared without the reverse transcriptase enzyme and was used as the no-reverse transcriptase negative control in the quantitative polymerase chain reaction (qPCR) protocol.

qPCR

cDNA was loaded into each well of a 96-well plate containing forward and reverse primers (primer sequences are given in supplemental online Table 2), 10 μl of 2$\times$ Power SYBR master mix (Thermo Fisher Scientific Life Sciences), and RNase-free H_2O to a final volume of 20 μl. The reaction was carried out in a Bio-Rad PTC-200 thermal cycler equipped with a Chromo4 real time detection system (Bio-Rad, Hercules, CA, http://www.bio-rad.com/), and the results were processed using Opticon Monitor 3 software (Bio-Rad). Each assay was performed in triplicate, averaged, and normalized to an endogenous control (β_2-microglobulin). Comparisons were made across experimental conditions using the $\Delta\Delta C_T$ method [44, 45]. Data are displayed as the $\log_2$ of the fold change in normalized expression. Primer sequences are included in supplemental online Table 1.

Electrophysiology and Fast Scan Cyclic Voltammetry

Neurons were grown and differentiated on coated glass coverslips. Glass coverslips were placed in an intracellular recording chamber, and neurons were observed using an Olympus BX51WI IR illumination DIC microscope with a 40$\times$ water-immersion objective (Olympus, Tokyo, Japan, http://www.olympus-ims.com). The recording chamber was continuously perfused at 2–3 ml/minute with artificial cerebrospinal fluid (aCSF) consisting of 125 mM NaCl, 2.5 mM KCl, 25 mM $NaHCO_3$, 1.25 mM NaH_2PO_4, 10 mM HEPES, 2 mM $CaCl_2$, 25 mM glucose, 1 mM $MgCl_2$, 1 mM ascorbic acid, and 2.4 mM sodium pyruvate (pH 7.4; 298 $mOsm^{-1}$). The aCSF was bubbled with 95% O_2 and 5% CO_2 for 30 minutes before use and heated to 37°C with an inline heater. Electrodes were pulled from borosilicate glass capillary tubes to a resistance of 3–7 MΩ and front-filled with a filtered internal solution consisting of 138 mM K-gluconate 5 mM KCl, 0.2 mM EGTA 5 mM HEPES, 2 mM $MgCl_2$, 0.4 mM GTP-Na, and 4 mM ATP-Na, 0.0001 mM $CaCl_2$ (pH 7.4; 290–300 $mOsm^{-1}$). We used both the whole cell patch clamp and the perforated patch clamp techniques to obtain access to cultured neurons. Perforated patch clamp was performed by backfilling the electrodes with internal solution containing 0.5–3 μg/ml gramicidin (Sigma-Aldrich). Upon achieving electrode-cell attachment, we waited 15–45 minutes for the gramicidin to perforate the patch of membrane underlying the electrode.

Electrical activity from the probed neuron was detected and amplified using an Axon MultiClamp 200B amplifier (Molecular Devices, Union City, CA, https://www.moleculardevices.com/) in current clamp mode. Data were recorded using AxoGraph software. Patches that did not reach a GΩ resistance seal or did not show a series resistance below 100 MΩ after 45 minutes in cell-attached mode were not analyzed further. Firing rates were calculated by counting the total number of action potentials in a specific window of time, during which we also observed pacemaking activity, and by dividing that number by the length of the corresponding time window. Spike width was calculated for all action potentials by finding the width of the action potential waveform in time between the points at which the action potential reached half of its maximum amplitude during the rising and the falling phases of each action potential. Interspike interval (ISI) was calculated by measuring the length of time between the end of one action potential and the beginning of the subsequent action potential. Coefficient of variation for ISI was calculated as the quotient of the standard deviation of ISIs divided by the mean.

For current injection experiments, a current-step protocol was used in which 1 second of depolarizing current was delivered to the neuron every 5 seconds. Each step increased the magnitude of the delivered current by 25 pA up to 200 pA (9 steps). After all 9 current injections were administered, the step protocol was repeated 2 more times. Labeling the recorded cell for ICC identification was achieved by filling the recording electrode with biocytin (1:1,000; Thermo Fisher Scientific Life Sciences). After the recording session, we stained the sample as described in the immunocytochemistry section. For visualization of biocytin, we stained with streptavidin 488 (1:500) for 1 hour at 37°C.

Catecholamine release was detected using fast-scan cyclic voltammetry using in-house fabricated carbon fiber microelectrodes [46]. The potential applied to the carbon fiber was ramped every 100 milliseconds from -0.4 V to 1.3 V (versus an Ag/AgCl reference electrode) and back down at 400 V/s. Electrodes were held at -0.4 V between voltage ramps. A 250-μm bipolar

stimulating electrode (FHC, Bowdoin, ME, http://www.fh-co.com/) placed adjacent to the carbon fiber electrode was used to stimulate neurotransmitter release. The current at the peak oxidation potential for catecholamines (approximately 0.65 V) was low-pass filtered at 2 KHz using LabView software (National Instruments, Austin, TX, http://www.ni.com). We identified three independent biological experiments in which the detected voltammetry signal after electrical stimulation significantly correlated with a standard cyclic voltammogram for dopamine (linear regression $r^2 \geq .75$) [47]. Analyses were performed in GraphPad Prism 6.04 for Windows (GraphPad Software, La Jolla, California USA, http://www.graphpad.com).

RESULTS

We induced differentiation of biPSCs to form DA cells using a modified version of the dual SMAD inhibition protocol as previously described (Fig. 1A) [41]. Baboon iPSCs were grown on MEFs until confluent (Fig. 1B), at which point we began the differentiation process. Neural rosettes could be visualized by day 8 (Fig. 1C, arrowheads). The neural rosettes continued to expand until day 15 (Fig. 1D). At this point, the cells were manually dissected from the culture dish and passaged. The neural rosettes reformed and expanded (Fig. 1E). Cells at this stage were predominantly positive for the early neuronal marker, NESTIN [48–50] (Fig. 1F), whereas few were positive for the late neuronal marker βIII-TUBULIN (Fig. 1G). Cells were then cultured in a maturation medium containing BDNF, GDNF, cAMP, and ascorbic acid but lacking the following reagents included in the differentiation media: FGF2, FGF8, and SHh (Fig. 1A, day 16 and forward). During maturation, the cells grew larger in soma diameter and sent out extensive processes, forming a dense network of interconnections (Fig. 1H, 1J, 1I, and 1K, arrows). High-magnification images of the maturation process are shown in Figure 1I and 1K and supplemental online Fig. 1.

Directed Differentiation Efficiently Converts biPSCs to Neurons

In humans, the SNc is further divided into distinct dorsal and ventral tiers that, unlike in the rodent, are interconnected by neurons that traverse the SNc [51]. Similar to the SNc, the ventral tegmental area (VTA), which lies immediately medial to the SNc, is also dopaminergic. These regional features are physiologically relevant because the VTA and the two tiers of the SNc exhibit differential susceptibilities to the pathology of PD [52–56]. Specifically, it is the ventral tier of the SNc that has demonstrated the greatest vulnerability to PD relative to both the SNc dorsal tier and the VTA [52, 53, 57]. There is currently no established marker that distinguishes dorsal-tier from ventral-tier SNc neurons in the human brain. However, in rodents, the inwardly rectifying K+ channel, GIRK2 (also known as KCNJ6), has been used as a marker to distinguish the SNc from the VTA [58–60]. The utility of this marker to distinguish SNc from VTA in humans has been called into question [61] because it has been shown to be expressed in both of these regions.

To clarify the appropriateness of this marker, we then validated antibodies for TH, GIRK2, FOXA2, and LMX1A in baboon midbrain tissue using a DAB-HRP protocol (supplemental online Fig. 2). We then immunostained baboon midbrain sections for GIRK2 and (TH), an upstream enzyme in the production of dopamine. We found that the baboon midbrain appears to have two tiers of TH^+ cells within the SNc (Fig. 2A) and, as in the human brain [51], the baboon SNc contains bridge neurons that traverse the gap between the two regions (Fig. 2A, arrow). Our results also show that in the baboon brain, GIRK2 is expressed in both the dorsal and ventral tiers of the SNc (Fig. 2B and 2C). We also found expression of GIRK2 in the baboon VTA (Fig. 2B and 2C), although the intensity of GIRK2 expression was lower in this region than in the SNc. This corroborates data from the Allen Brain Institute showing a 3.75-fold upregulation in *GIRK2* transcript in the SNc relative to the VTA in humans [62] (http://human.brain-map.org/). Thus, the pattern of GIRK2 expression in the baboon brain is analogous to that in humans [61], with GIRK2 being expressed in both the dorsal and ventral tiers of the SNc as well as in the VTA, although to a reduced extent compared with that observed in the SNc.

We next used ICC to confirm the identity of our biPSC-derived neurons. Fully differentiated cells were assayed for expression of TH. After differentiation, 25.18% (SD, 12.6%) of all cells were positive for the neuronal marker βIII-TUBULIN, 13.63% (SD, 4.9%) were TH^+, and 9.09% (SD, 2.5%) were positive for both TH^+ and βIII-$TUBULIN^+$ (Fig. 2D and 2E). Of the βIII-$TUBULIN^+$ neurons, 68.4% (SD, 26.8%) expressed TH (Fig. 2G, right axis). At the end of the maturation period (day 50), we found that 74.4% (SD, 29.9%) of all cells expressed βIII-TUBULIN, 55.1% (SD, 22.3%) of all cells were βIII-TUBULIN and TH double-positive (supplemental online Fig. 3A), and 73.16% (SD, 1.68%) of all βIII-$TUBULIN^+$ neurons were TH^+ (supplemental online Fig. 3A). We also found that the biPSC-derived neurons showed a staining pattern similar to that observed in cells that reside within the baboon SNc (Fig. 2F). We next interrogated biPSC-derived dopaminergic neurons for the presence of GIRK2. Our results show that directed differentiation produced βIII-$TUBULIN^+$ cells that were $GIRK2^+$ (supplemental online Fig. 3B–3E) as well as TH^+ cells that were $GIRK2^-$ (Fig. 2H, arrowhead) or $GIRK2^+$ (Fig. 2H and 2I, arrows).

biPSC-Derived Neurons Upregulate Genes Characteristic of Dopaminergic Neurons

We analyzed gene expression using RT-qPCR. We selected a battery of genes that have been previously shown to be upregulated in neurons, including early neural marker *PAX6* [63]; late neural marker *βIII-TUBULIN*; and genes shown to be upregulated in midbrain dopamine neurons, including *FOXA2* [64, 65], *LMX1A* [66–68], *NURR1* [69], and *TH* [70]. We found that relative to undifferentiated biPSCs, in vitro derived neurons had low levels of expression of both *OCT4* and *NANOG* (Fig. 3A) and concomitantly increased expression of transcripts indicative of dopamine neurons throughout the differentiation process (Fig. 3).

Electrophysiological Characterization of biPSC-Derived Neurons

After maturation, we used both whole cell and perforated patch protocols in which electrical access to the cell was gained with minimal physical perturbation of the cell membrane [71]. Using these techniques, we obtained sufficient access for electrophysiological recordings (supplemental online Fig. 5A). We achieved access to 11 biPSC-derived neurons. Endogenous dopamine cells in the human midbrain display spontaneous

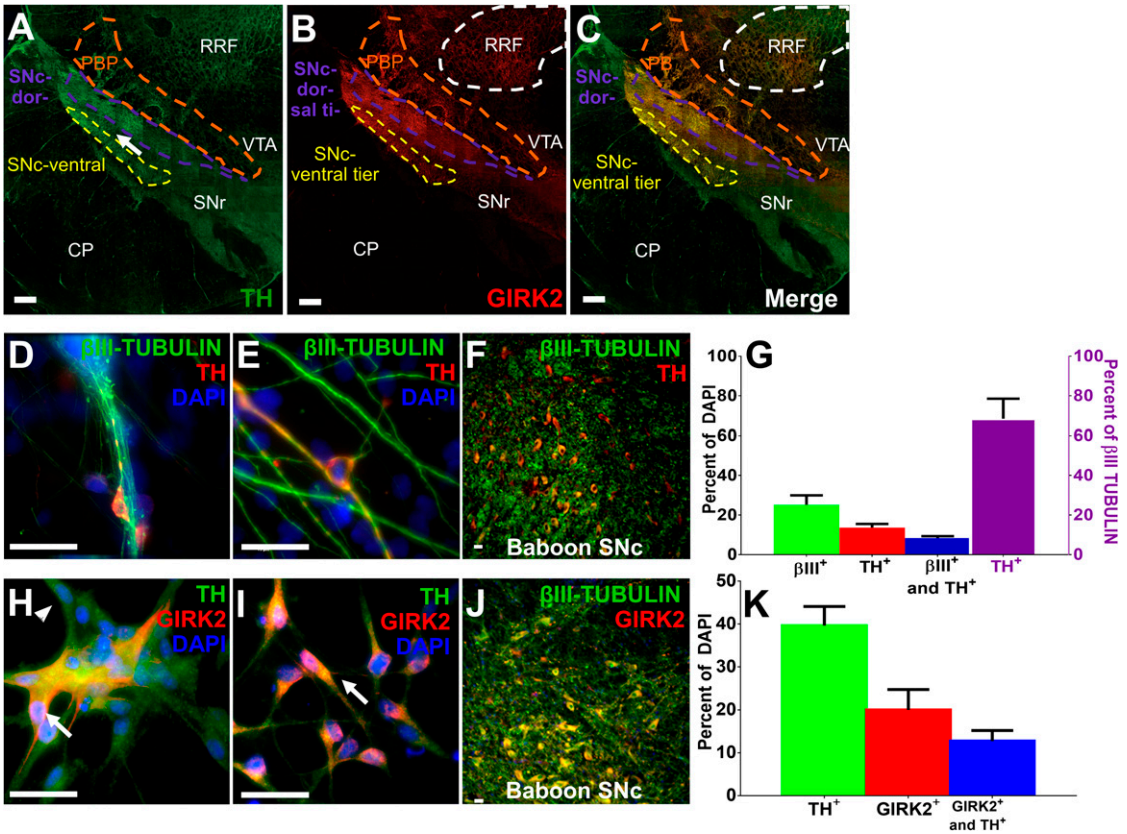

Figure 2. Expression of midbrain and dopaminergic markers in neurons derived from baboon fibroblast-derived induced pluripotent stem cells (biPSCs). **(A):** TH expression in the baboon midbrain identifies two tiers within the SNc: the dorsal tier (outlined in blue) and the ventral tier (outlined in yellow). There are TH-positive processes from putative bridge cells that traverse the gap between these two tiers (arrow). **(B):** GIRK2 is expressed in both tiers of the SNc: the RRF and the VTA. **(C):** Merged image of images A and B. **(D, E):** After maturation, biPSC-derived neurons expressed TH and βIII-TUBULIN. **(F):** The neurons in D and E represent the expression pattern of the neurons of the baboon SNc. **(G):** Cell counts show that 25.18% of the cells were converted to neurons, greater than 13.63% of the cells expressed TH, and 68.4% of the βIII-TUBULIN+ neurons expressed TH (right axis). **(H, I):** biPSC-derived TH+ cells that are negative for GIRK2 (arrowhead). **(I):** biPSC-derived cells that coexpress GIRK2 and TH (arrows). **(J):** Cells of the baboon SNc also express GIRK2. **(K):** Cell counts show that about 12.73% of cells expressed both GIRK2 and TH. Scale bar in **A–C** = 500 μm. Scale bars = 25 μm **(D–K)**. Abbreviations: CP, cerebral peduncle; DAPI, 4′,6-diamidino-2-phenylindole; PBP, parabrachial pigmented area; RRF, retrorubral field; SNc, substantia nigra pars compacta; SNr, substantia nigra pars reticulata; VTA, ventral tegmental area.

rhythmic firing of action potentials from 2 to 10 Hz [72, 73]. We observed spontaneous pacemaking activity in 11 biPSC-derived neurons (1302131, 1302132, 130310, 1513191, 1503192, 150521, 1505213, 1505214, 1511035, 1512175, and 1512177) (Fig. 4A–4C). Another characteristic of dopamine cells is the duration of the action potential. This parameter is calculated by measuring the width of an action potential at the point at which it has reached half of its maximum amplitude (spike half-maximal width). Dopamine neurons of the SNc show a spike half-maximal width greater than 0.8 milliseconds in humans in vivo [73] and greater than 1.5 milliseconds in rodents in vivo [74] and greater than 2.5 milliseconds in rodents in vitro [75]. In the 11 neurons from which we recorded spontaneous activity, we observed an average spike width of 4.98 milliseconds (range, 1.5–10.3 milliseconds) in duration (Fig. 4B and 4C). We also measured the ISIs of pacemaking activity. In these spontaneously active neurons, we found that the average ISI was 0.62 seconds (Fig. 4C). The frequencies observed in biPSC-derived neurons are consistent with the 2–5 Hz observed in dopamine cells in humans [73] and rodents [76] in vivo. The coefficients of variation of the ISIs (a measurement of regularity in spike frequency) were between 0.22 (consistent frequency in spiking) and 1.11 (variable frequency in spiking) (Fig. 4C), which is consistent with values observed in dopamine neurons from both rodents [77] and primates [78] in vitro. We also verified that these electrophysiological properties are expressed in dopamine neurons by neurons with biocytin during electrophysiological recordings. After the recording session, filled neurons can be identified after fixation, permeabilization, and incubation in streptavidin-488. We found that labeled biPSC-derived neurons that expressed a $>$2-millisecond spike width, a 1- to 5-Hz firing frequency, and spike frequency adaptation using biocytin and found that these neurons also expressed TH (supplemental online Fig. 4).

We also found that depolarizing current elicited high-frequency action potential firing in three neurons (Fig. 5A, 5B; supplemental online Fig. 4). In one of these neurons (130310), increasing the intensity of the depolarizing current increased the rate of action potential firing in a linear fashion (Fig. 5B). However, for two neurons (1302131, 1512175), increasing the current could not drive the firing rate past 22 Hz (Fig. 5B; supplemental online Fig. 4). Electrophysiological recordings in rodents show that dopamine neurons exhibit a phenomenon known as spike frequency adaptation, in which bursts of action potentials begin with a high frequency but end with a reduced frequency [79]. Two of the

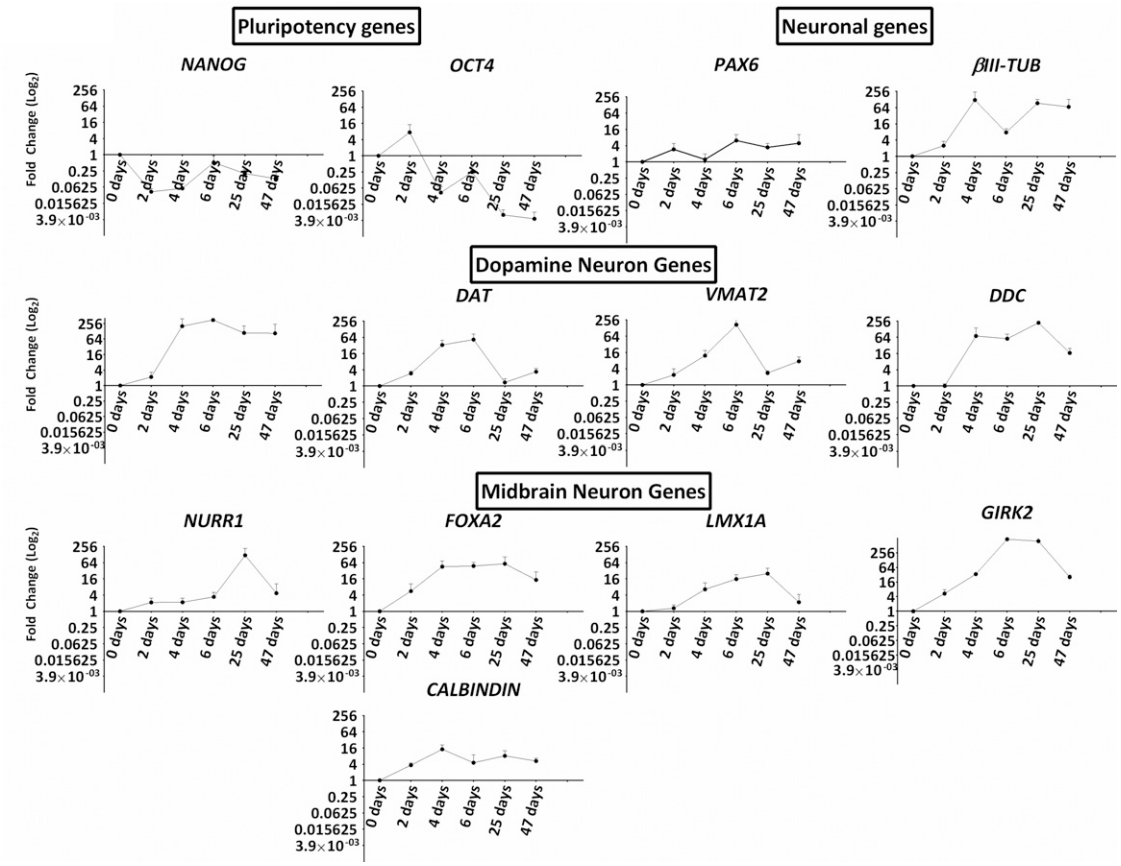

Figure 3. Real-time quantitative polymerase chain reaction (qPCR) of neurons derived from baboon fibroblast-derived induced pluripotent stem cells (biPSCs). Fold change in expression calculated from the $\Delta\Delta C_T$ of average of three technical replicates of a qPCR reaction. Reactions were carried out using cDNA made from RNA isolated at the indicated number of days after initiating the differentiation process and from RNA isolated from the parent biPSC cell line. Data are presented as the $\log_2$ of the fold change in expression of the indicated mRNA transcript. Reduction of *NANOG* and *OCT4* indicates a loss of pluripotency during differentiation. Upregulation of *PAX6* and *βIII-TUBULIN* indicates differentiation toward the neuronal fate. Upregulation of *TH*, *DAT*, *VMAT2*, and *DDC* indicates the dopamine neuron phenotype, and increased expression of *FOXA2*, *LMX1A*, *GIRK2* and *CALBINDIN* indicates the phenotype of dopamine neurons from the ventral midbrain specifically.

biPSC-derived dopamine neurons (1302131 and 1512175) showed a similar spike frequency adaptation in which the frequency of action potentials was reduced throughout the duration of the current injection (Fig. 5C; supplemental online Fig. 4), but the other neuron (130310) did not demonstrate this adaptation as the rates did not decrease through the duration of the current injection (Fig. 5D). Lastly, dopamine cells in the human SNc also express an inhibitory autoreceptor, D2R, and dopamine binding to D2R can lead to a reduction in dopamine cell activity [80]. We found that the depolarization-induced high-frequency activity depicted in Figure 5A could be reduced with administration of the D2R agonist, quinpirole (supplemental online Fig. 5B).

Using fast-scan cyclic voltammetry, we found that electrical stimulation of biPSC cultures evoked a signal matching the electrochemical signature for dopamine (linear regression relative to a standard cyclic voltammogram for dopamine, $r^2 \geq .75$; $n = 3$ independent experiments) (Fig. 5E, 5F; supplemental online Fig. 6).

Discussion

To ensure safety and efficacy of cell-based treatments for PD or other neurodegenerative diseases, many parameters need to be optimized. These parameters include the optimal route of delivery of cells, the ability of cells to persist and proliferate after transplantation, the effect of any immune reaction to the transplanted cells, the extent of alleviation of the condition for which the transplanted cells are used, the precise location of the graft site, and the extent to which the transplanted cells elicit off-target effects (e.g., graft-induced dyskinesias or tumorigenesis). To be truly informative, this must be accomplished in clinically relevant animal models.

Neuronal differentiation from pluripotent stem cells has been described for several nonhuman primate species, including marmosets [18, 81], rhesus macaques [82–84], and crab-eating macaques [85]. This is the first study to describe dopaminergic differentiation from the olive baboon (*P. anubis*). Baboons are a favored nonhuman primate for transplant studies. The baboon provides one of the most accurate animal models of the human immune system [32, 86–91], possessing genes encoding all four subclasses of IgG. Furthermore, IgG proteins in the baboon share a 90% sequence identity with human IgG proteins at the peptide level [86]. Humans and baboons also both display an age-related increase in autoimmune disorders, presumably stemming from an increased recognition of autoantigens [88]. These characteristics, in combination with neuroanatomical congruencies between baboon and human, render the baboon an ideal,

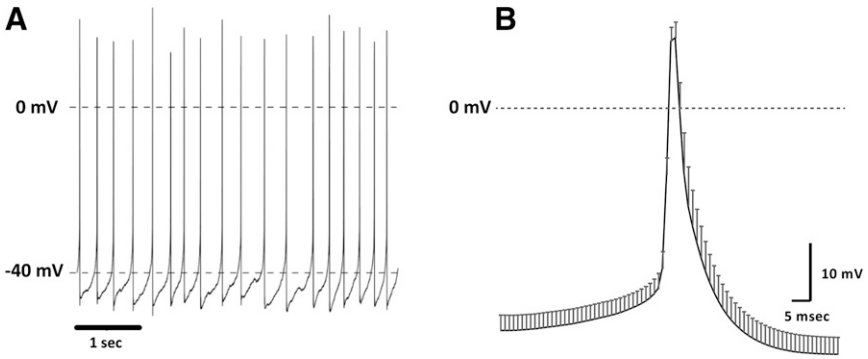

C

Cell	Average Spike Width (msec)	Pacemaking Frequency (Hz)	Average ISI (sec)	ISI Coefficient of Variation
130231	2.57	1.82	0.80	0.63
130232	3.07	2.00	0.50	0.94
130310	3.11	5.72	0.32	0.97
1503191	1.59	2.01	1.27	1.11
1503192	5.46	1.99	0.77	0.69
1505211	7.20	13.00	0.08	0.46
1505213	7.75	4.60	0.23	0.66
1505214	10.30	6.00	0.17	0.44
1511035	3.81	0.97	1.45	0.81
1512175	5.09	6.02	1.66	0.22
1512177	4.73	2.50	0.40	0.51
Average	**5.00**	**4.41**	**0.73**	**0.68**

Figure 4. Characterization of pacemaking activity in neurons derived from baboon fibroblast-derived induced pluripotent stem cells (biPSCs). **(A):** Tonic spontaneous action potentials from a biPSC-derived neuron recorded in current clamp. **(B):** The average action potential trace from 11 neurons (dark line). Error bars in gray represent SEM. **(C):** Average spike widths, average firing rates, average ISIs, and coefficients of variation from 11 neurons demonstrating spontaneous activity. ISIs were between 0.08 and 1.66 seconds in length. The average ISIs were calculated by averaging the length of time between each action potential and a subsequent action potential during pacemaking activity. The coefficient of variation of the ISIs (a measure of regularity of pacemaking) was calculated by taking the quotient of the SD of the ISIs divided by the mean of the ISIs. Abbreviation: ISI, interspike interval.

clinically relevant model in which to develop cell-based therapeutic approaches for the treatment of PD.

A key initial feature of any model to be used for testing cell-based therapies for PD is the ability to faithfully derive the requisite cell type —and for PD the relevant cell type is dopaminergic neurons. The first protocol describing differentiation of DA cells from pluripotent stem cells was published in 2004 [16]. Similar to other protocols for derivation of DA neurons [40, 41, 58, 66, 67, 92–99], the directed differentiation protocol in that study used FGF8 and SHh to recapitulate the in vivo developmental exposure to these molecules in the mesencephalon [100, 101]. In an effort to produce a higher yield of dopaminergic neurons, many laboratories have since modified this protocol or developed novel protocols with varying degrees of success, resulting in a diverse array of published differentiation protocols [40, 41, 58, 66, 67, 92–99, 102], each demonstrating varying levels of efficiency. Recently, a molecular agonist of the WNT signaling pathway, CHIR99021, was used to induce expression of *LMX1A*, and this resulted in 75% purity of $TH^+/\beta III\text{-}TUBULIN^+$ cells [41]. Using a slightly modified version of this protocol, we were able to differentiate baboon iPSCs into neurons with a yield of 68.4% (SD, 26.7%) $TH^+/\ \beta III\text{-}TUBULIN^+$ cells (13.63% [SD, 5.0%] of all cells). Previous publications describing differentiation of dopaminergic neurons from nonhuman primate pluripotent cells have typically not reported differentiation efficiencies [58, 81, 82, 85, 96], with the exception of two cases in which dopaminergic neurons were derived from crab-eating macaque iPSCs at an efficiency of 10% TH^+ cells among all cells [83, 84], which is similar to our results. A third study of crab-eating macaque iPSCs reported that 30% of their $\beta III\text{-}TUBULIN^+$ cells were TH^+ [103].

GIRK2 expression within DA cells is widely believed to distinguish the SNc-type DA neuron from the VTA-type DA neuron [41, 58, 66]. Support for this comes from work showing that $GIRK2^+$ cells in a mouse transplantation experiment will innervate the striatum, whereas $GIRK2^-$ cells will not innervate the striatum [3]. However, the validity of GIRK2 as a specific marker for SNc-type cells has been refuted in the human brain because $GIRK2^+$ cells are found in both the SNc and the VTA, with GIRK2 expression being strongest in the SNc [61]. Here, we report the first study to investigate GIRK2 expression in the baboon brain. We found that GIRK2 is expressed in both the VTA and the SNc in the baboon brain, but with the strongest expression in the lateral portions of the SNc, recapitulating the pattern observed in the human brain. Thus, the baboon cytoarchitecture reported here reflects that observed in the human midbrain, further validating the baboon as an appropriate transplantation model for PD. Nevertheless, it remains likely that more accurate markers will need to be identified to unequivocally distinguish these two closely related cell types.

We also demonstrated electrophysiological function of biPSC-derived neurons manifest as pacemaking activity, as well as current-induced high-frequency action potential firing. We found that our neurons fired spontaneous action potentials with spike widths and frequencies congruent with those seen in both primates and rodents. When we injected current into biPSC-derived neurons, they fired at frequencies higher than those typically observed in slice recordings of the Sprague-Dawley albino rat substantia nigra, which usually do not fire faster than 8–15 Hz [72, 76]. The increased firing rate we observed in biPSC-derived

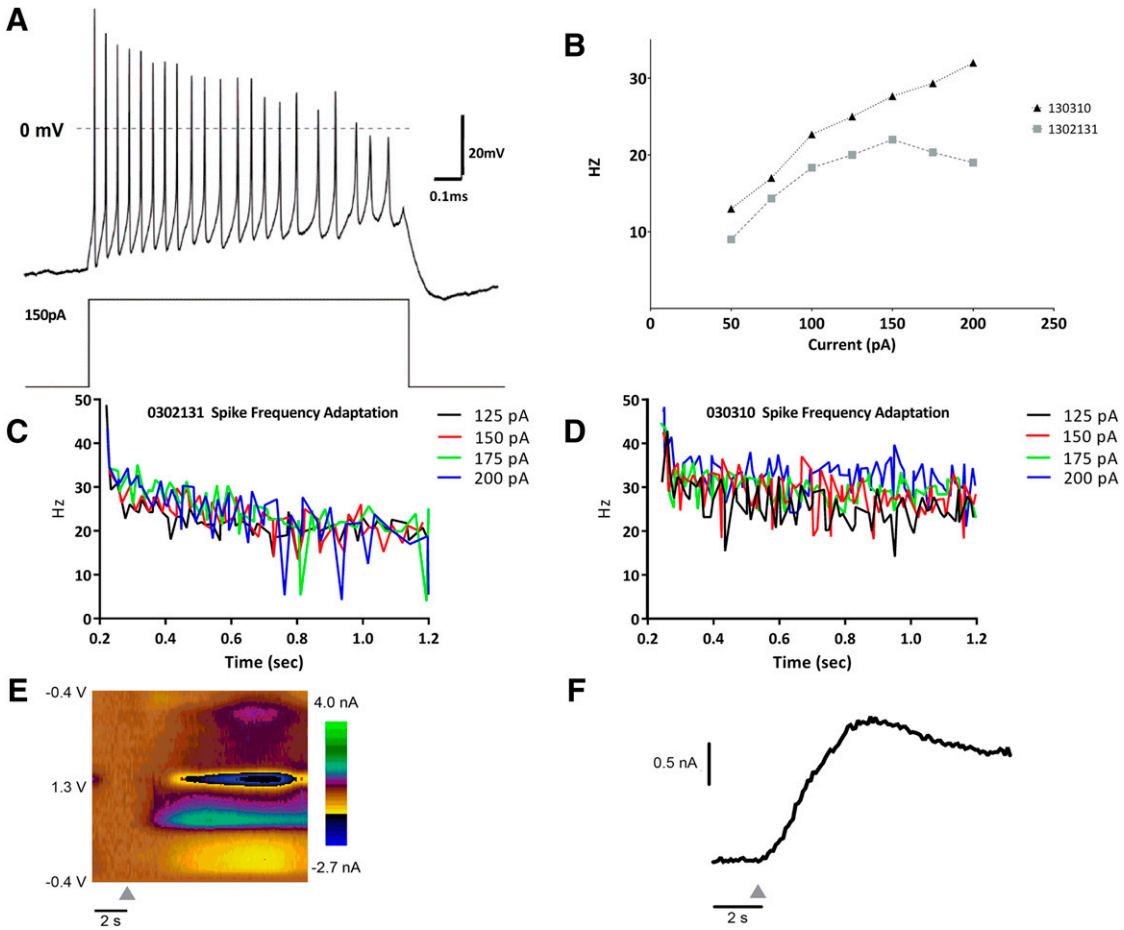

Figure 5. Characterization of stimulation-induced action potential firing of neurons derived from baboon fibroblast-derived induced pluripotent stem cells (biPSCs). **(A):** Representative current clamp recording from one cell during a 150-pA current injection. The cell fired with a high frequency at the onset of current injection but slowed through the duration of the injection. **(B):** Frequency versus current curve of two different cells from which we observed stimulation-induced action potentials. Each trace represents the average firing rate of three repetitions at each current intensity for each cell. With increasing current intensity, 130310 increased its firing rate up to 32 Hz. The firing rate of 1302131 did not exceed 22.0 Hz despite increasing current intensity. **(C, D):** The firing rates of 1302131 and 130310 as a function of current and time; each trace represents a different current intensity. 1302131 reduced firing rate throughout the duration of the pulse, suggestive of spike frequency adaptation. Voltammetry recording performed on cultured neurons illustrating catecholamine release after a 5-pulse, 4-Hz, 300-μA electrical stimulation (gray triangle). **(E):** Impulse-dependent catecholamine release. Two-dimensional pseudocolor plots of cyclic voltammograms (*y*-axis) over time (*x*-axis). Cultured cells were pretreated with 100 μM L-dopa for 30 minutes before recordings. Voltage was ramped from -0.4 V up to +1.3 V and back down to -0.4 V every 100 milliseconds. Detected signal matched a standard template of dopamine with an $r^2 > .75$. **(F):** Current at the peak oxidation potential for dopamine (approximately 0.65 V) is plotted as a function of time. Gray triangle denotes when electrical stimulation (10 Hz, 30 p, 300 μA) was applied.

neurons relative to that commonly seen in the rodent may reflect species differences between primates and rodents. To our knowledge, no one has characterized the electrophysiology of the baboon substantia nigra in vitro. However, studies have shown that primates such as the crab-eating macaque (*Macaca fascicularis*) possess SNc neurons capable of firing at rates of 20–60 Hz in vivo [104, 105], whereas the SNc cells of the common marmoset (*Callithrix jacchus*) release a maximal amount of dopamine in the striatum when firing at 20 Hz [106, 107]. These rates differ from the optimal firing rate for DA release in the rat, of which the fastest measured is 14 Hz [106]. The coefficient of variation of the ISIs of our neurons ranged between 0.22 (consistent frequency in firing) and 1.1 (variable frequency in spiking), with an average at 0.75. These values fall closely in line with those observed in dopamine neurons of the awake and behaving rhesus macaque, whose coefficient of variation varies between 0.4 and 1.0 [78]. Collectively, these data suggest that primates require higher firing frequencies for peak dopamine release than rodents, which would be consistent with the frequencies we observed in biPSC-derived neurons.

By employing voltammetry recordings in our characterization of biPSC neurons, we qualitatively demonstrated that biPSC neuronal cultures are capable of impulse-dependent catecholamine release. To our knowledge, this is the first time cyclic voltammetry has been adapted for probing catecholamine release in cultured neurons differentiated from pluripotent stem cells. Future experiments will systematically identify the optimal stimulation parameters for evoking catecholamine release from biPSC neuronal cultures. Importantly, we demonstrate that our biPSC derived neurons are capable of appropriately responding to stimulation by not only firing action potentials but also by neurotransmitter release and that they therefore represent fully functional neurons.

Our data confirm that the positive expression of common dopaminergic markers, such as TH alone, is not sufficient to unequivocally identify a fully functional dopamine cell because 68.4% of the neurons we generated expressed TH. However, only one of the seven cells probed displayed all electrophysiological characteristics generally considered representative of dopaminergic neurons. The full range of properties of dopaminergic neurons remains to be defined, especially with respect to distinguishing dopaminergic neurons of the SNc from those of the VTA. An advantage of the baboon model is that it will facilitate a rigorous characterization of stem cell-derived neurons, including direct comparisons with characteristics of the equivalent endogenous neurons in the primate brain. The ability to unambiguously separate neurons with characteristics of distinct brain regions will be essential for the optimization of cell transplantation therapies and their subsequent translation into the clinic.

Conclusion

Toward our goal of establishing the baboon as a useful preclinical model for evaluating stem cell-derived therapies for PD, we demonstrate here that biPSCs can be efficiently differentiated into DA cells. These baboon DA cells express *PAX6, βIII-TUBULIN, FOXA2, LMX1A, NURR1,* and *TH,* consistent with the expression pattern of a human midbrain DA cell. They also fire action potentials spontaneously at 2–5 Hz as well as displaying high-frequency (20–30 Hz) firing activity and catecholamine release when subjected to electrical stimulation. Thus, these cells differentiate into neurons that demonstrate both the expected cell type-specific gene expression pattern and the functionality of neurons found in the human brain. The ability we demonstrate here to generate biPSC-derived DA neurons and to study and manipulate these cells in culture, in conjunction with the potential to transplant these cells into brains of living baboons, establishes the baboon as a valuable model for testing and optimizing the safety and efficacy of pluripotent stem cell-based therapeutic approaches for the treatment of PD or other neurodegenerative diseases.

Acknowledgments

This study was supported by a gift from the Robert and Helen Kleberg Foundation to J.R.M., by National Institutes of Health Grants MH079276 and DA030530 to C.A.P. and Grant DA033386 to M.J.W., by National Institute of General Medical Sciences Research Initiative for Scientific Enhancement GM60655 to J.A.G. and D.V.S., and by National Science Foundation Grant HRD1249284 to J.A.G.

Author Contributions

D.A.G.: conception and design, collection and/or assembly of data, data analysis and interpretation, manuscript writing, final approval of manuscript; D.V.S., M.J.W.: collection and/or assembly of data, data analysis and interpretation, manuscript writing, final approval of manuscript; J.A.G.: collection and/or assembly of data, final approval of manuscript; J.R.M.: financial support, provision of study material or patients, manuscript writing, final approval of manuscript; C.A.P.: financial support, data analysis and interpretation, manuscript writing, final approval of manuscript; C.S.N.: conception and design, financial support collection and/or assembly of data, data analysis and interpretation, manuscript writing, final approval of manuscript.

Disclosure of Potential Conflicts of Interest

The authors indicated no potential conflicts of interest.

References

1 Carlsson A. The occurrence, distribution and physiological role of catecholamines in the nervous system. Pharmacol Rev 1959;11:490–493.

2 Parkinson J. An Essay on the Shaking Palsy. London: Whittingham and Rowland, 1817.

3 Thompson L, Barraud P, Andersson E et al. Identification of dopaminergic neurons of nigral and ventral tegmental area subtypes in grafts of fetal ventral mesencephalon based on cell morphology, protein expression, and efferent projections. J Neurosci 2005;25:6467–6477.

4 Olanow CW, Kordower JH, Freeman TB. Fetal nigral transplantation as a therapy for Parkinson's disease. Trends Neurosci 1996;19:102–109.

5 Thompson LH, Grealish S, Kirik D et al. Reconstruction of the nigrostriatal dopamine pathway in the adult mouse brain. Eur J Neurosci 2009;30:625–638.

6 Freed CR, Greene PE, Breeze RE et al. Transplantation of embryonic dopamine neurons for severe Parkinson's disease. N Engl J Med 2001;344:710–719.

7 Olanow CW, Goetz CG, Kordower JH et al. A double-blind controlled trial of bilateral fetal nigral transplantation in Parkinson's disease. Ann Neurol 2003;54:403–414.

8 Bjorklund A, Kordower JH. Cell therapy for Parkinson's disease: What next? Mov Disord 2013;28:110–115.

9 Lindvall O, Björklund A. Cell therapy in Parkinson's disease. NeuroRx 2004;1:382–393.

10 Politis M, Wu K, Loane C et al. Serotonergic neurons mediate dyskinesia side effects in Parkinson's patients with neural transplants. Sci Transl Med 2010;2:38ra46.

11 Carta M, Carlsson T, Muñoz A et al. Role of serotonin neurons in the induction of levodopa- and graft-induced dyskinesias in Parkinson's disease. Mov Disord 2010;25(suppl 1):S174–S179.

12 Politis M, Oertel WH, Wu K et al. Graft-induced dyskinesias in Parkinson's disease: High striatal serotonin/dopamine transporter ratio. Mov Disord 2011;26:1997–2003.

13 Guha P, Morgan JW, Mostoslavsky G et al. Lack of immune response to differentiated cells derived from syngeneic induced pluripotent stem cells. Cell Stem Cell 2013;12:407–412.

14 Araki R, Uda M, Hoki Y et al. Negligible immunogenicity of terminally differentiated cells derived from induced pluripotent or embryonic stem cells. Nature 2013;494:100–104.

15 Kiskinis E, Eggan K. Progress toward the clinical application of patient-specific pluripotent stem cells. J Clin Invest 2010;120:51–59.

16 Perrier AL, Tabar V, Barberi T et al. Derivation of midbrain dopamine neurons from human embryonic stem cells. Proc Natl Acad Sci USA 2004;101:12543–12548.

17 Kocerha J, Xu Y, Prucha MS et al. A two years longitudinal study of transgenic Huntington disease monkey. BMC Neurosci 2014;15:36.

18 Farnsworth SL, Qiu Z, Mishra A et al. Directed neural differentiation of induced pluripotent stem cells from non-human primates. Exp Biol Med (Maywood) 2013;238:276–284.

19 Wianny F, Bourillot PY, Dehay C. Embryonic stem cells in non-human primates: An overview of neural differentiation potential. Differentiation 2011;81:142–152.

20 Daadi MM, Barberi T, Shi Q et al. Nonhuman primate models in translational regenerative medicine. Stem Cells Dev 2014;23(suppl 1):83–87.

21 Daadi MM, Grueter BA, Malenka RC et al. Dopaminergic neurons from midbrain-specified human embryonic stem cell-derived neural stem cells engrafted in a monkey model of Parkinson's disease. PLoS One 2012;7:e41120.

22 Hallett PJ, Deleidi M, Astradsson A et al. Successful function of autologous iPSC-derived dopamine neurons following transplantation in a non-human primate model of Parkinson's disease. Cell Stem Cell 2015;16:269–274.

23 Bédard P, Larochelle L, Parent A et al. The nigrostriatal pathway: A correlative study based on neuroanatomical and neurochemical criteria in the cat and the monkey. Exp Neurol 1969;25: 365–377.

24 Cook DJ, Tymianski M. Nonhuman primate models of stroke for translational neuroprotection research. Neurotherapeutics 2012; 9:371–379.

25 Schoenemann PT, Sheehan MJ, Glotzer LD. Prefrontal white matter volume is disproportionately larger in humans than in other primates. Nat Neurosci 2005;8:242–252.

26 D'Ambrosio AL, Sughrue ME, Mocco J et al. A modified transorbital baboon model of reperfused stroke. Methods Enzymol 2004; 386:60–73.

27 Duong TQ. Diffusion tensor and perfusion MRI of non-human primates. Methods 2010;50:125–135.

28 Sakai F, Meyer JS, Yamaguchi F et al. 133Xe inhalation method for measuring cerebral blood flow in conscious baboons. Stroke 1979;10:310–318.

29 Herculano-Houzel S. Scaling of brain metabolism with a fixed energy budget per neuron: Implications for neuronal activity, plasticity and evolution. PLoS One 2011;6:e17514.

30 Hardman CD, Henderson JM, Finkelstein DI et al. Comparison of the basal ganglia in rats, marmosets, macaques, baboons, and humans: Volume and neuronal number for the output, internal relay, and striatal modulating nuclei. J Comp Neurol 2002;445:238–255.

31 Moore AR, Filipovic R, Mo Z et al. Electrical excitability of early neurons in the human cerebral cortex during the second trimester of gestation. Cereb Cortex 2009;19:1795–1805.

32 McFarlane D, Wolf RF, McDaniel KA et al. Age-associated alteration in innate immune response in captive baboons. J Gerontol A Biol Sci Med Sci 2011;66:1309–1317.

33 Stacy S, Pasquali A, Sexton VL et al. An age-old paradigm challenged: Old baboons generate vigorous humoral immune responses to LcrV, a plague antigen. J Immunol 2008;181:109–115.

34 Murthy KK, Salas MT, Carey KD et al. Baboon as a nonhuman primate model for vaccine studies. Vaccine 2006;24:4622–4624.

35 Perry DL, Bollinger L, White GL. The Baboon (Papio spp.) as a model of human Ebola virus infection. Viruses 2012;4:2400–2416.

36 Vandeberg JL, Williams-Blangero S, Tardiff SD. The baboon in biomedical research. In: RH Tuttle, ed. Developments in Primatology: Progress and Prospects. New York, NY: Springer, 2009.

37 Navara CS, Hornecker J, Grow D et al. Derivation of induced pluripotent stem cells from the baboon: A nonhuman primate model for preclinical testing of stem cell therapies. Cell Reprogram 2013;15:495–502.

38 Simerly CR, Navara CS, Castro CA et al. Establishment and characterization of baboon embryonic stem cell lines: An Old World Primate model for regeneration and transplantation research. Stem Cell Res (Amst) 2009;2: 178–187.

39 Chang T-C, Liu YG, Eddy CA et al. Derivation and characterization of novel nonhuman primate embryonic stem cell lines from in vitrofertilized baboon preimplantation embryos. Stem Cells Dev 2011;20:1053–1062.

40 Chambers SM, Fasano CA, Papapetrou EP et al. Highly efficient neural conversion of human ES and iPS cells by dual inhibition of SMAD signaling. Nat Biotechnol 2009;27:275–280.

41 Kriks S, Shim JW, Piao J et al. Dopamine neurons derived from human ES cells efficiently engraft in animal models of Parkinson's disease. Nature 2011;480:547–551.

42 Schneider CA, Rasband WS, Eliceiri KW. NIH Image to ImageJ: 25 years of image analysis. Nat Methods 2012;9:671–675.

43 McRitchie DA, Cartwright H, Pond SM et al. The midbrain dopaminergic cell groups in the baboon Papio ursinus. Brain Res Bull 1998;47:611–623.

44 Livak KJ, Schmittgen TD. Analysis of relative gene expression data using real-time quantitative PCR and the 2(-Delta Delta C(T)) Method. Methods 2001;25:402–408.

45 Cikos S, Bukovská A, Koppel J. Relative quantification of mRNA: comparison of methods currently used for real-time PCR data analysis. BMC Mol Biol 2007;8:113.

46 Clark JJ, Sandberg SG, Wanat MJ et al. Chronic microsensors for longitudinal, subsecond dopamine detection in behaving animals. Nat Methods 2010;7:126–129.

47 Wanat MJ, Kuhnen CM, Phillips PE. Delays conferred by escalating costs modulate dopamine release to rewards but not their predictors. J Neurosci 2010;30:12020–12027.

48 Dahlstrand J, Lardelli M, Lendahl U. Nestin mRNA expression correlates with the central nervous system progenitor cell state in many, but not all, regions of developing central nervous system. Brain Res Dev Brain Res 1995; 84:109–129.

49 Lendahl U, Zimmerman LB, McKay RDG. CNS stem cells express a new class of intermediate filament protein. Cell 1990;60:585–595.

50 Kawaguchi A, Miyata T, Sawamoto K et al. Nestin-EGFP transgenic mice: Visualization of the self-renewal and multipotency of CNS stem cells. Mol Cell Neurosci 2001;17:259–273.

51 McRitchie DA, Hardman CD, Halliday GM. Cytoarchitectural distribution of calcium binding proteins in midbrain dopaminergic regions of rats and humans. J Comp Neurol 1996;364: 121–150.

52 Hirsch E, Graybiel AM, Agid YA. Melanized dopaminergic neurons are differentially susceptible to degeneration in Parkinson's disease. Nature 1988;334:345–348.

53 Gibb WRG, Lees AJ. Anatomy, pigmentation, ventral and dorsal subpopulations of the substantia nigra, and differential cell death in Parkinson's disease. J Neurol Neurosurg Psychiatry 1991;54:388–396.

54 Fuxe K. Evidence for the existence of monoamine neurons in the central nervous system. Zeitschrift für Zellforschung und Mikroskopisch 1965;5996:573–596.

55 Andén N-E, Hfuxe K, Hamberger B et al. A quantitative study on the nigro-neostriatal dopamine neuron system in the rat. Acta Physiol Scand 1966;67:306–312.

56 Swanson LW. The projections of the ventral tegmental area and adjacent regions: A combined fluorescent retrograde tracer and immunofluorescence study in the rat. Brain Res Bull 1982;9:321–353.

57 Gibb WRG. Melanin, tyrosine hydroxylase, calbindin and substance P in the human midbrain and substantia nigra in relation to nigrostriatal projections and differential neuronal susceptibility in Parkinson's disease. Brain Res 1992;581:283–291.

58 Xi J, Liu Y, Liu H et al. Specification of midbrain dopamine neurons from primate pluripotent stem cells. STEM CELLS 2012;30:1655–1663.

59 Gaillard A, Decressac M, Frappé I et al. Anatomical and functional reconstruction of the nigrostriatal pathway by intranigral transplants. Neurobiol Dis 2009;35:477–488.

60 Schein JC, Hunter DD, Roffler-Tarlov S. Girk2 expression in the ventral midbrain, cerebellum, and olfactory bulb and its relationship to the murine mutation weaver. Dev Biol 1998;204:432–450.

61 Reyes S, Fu Y, Double K et al. GIRK2 expression in dopamine neurons of the substantia nigra and ventral tegmental area. J Comp Neurol 2012;520:2591–2607.

62 Hawrylycz MJ, Lein ES, Guillozet-Bongaarts AL et al. An anatomically comprehensive atlas of the adult human brain transcriptome. Nature 2012;489:391–399.

63 Chung CY, Seo H, Sonntag KC et al. Cell type-specific gene expression of midbrain dopaminergic neurons reveals molecules involved in their vulnerability and protection. Hum Mol Genet 2005;14:1709–1725.

64 Ang SL. Transcriptional control of midbrain dopaminergic neuron development. Development 2006;133:3499–3506.

65 Lin W, Metzakopian E, Mavromatakis YE et al. Foxa1 and Foxa2 function both upstream of and cooperatively with Lmx1a and Lmx1b in a feedforward loop promoting mesodiencephalic dopaminergic neuron development. Dev Biol 2009;333:386–396.

66 Friling S, Andersson E, Thompson LH et al. Efficient production of mesencephalic dopamine neurons by Lmx1a expression in embryonic stem cells. Proc Natl Acad Sci USA 2009; 106:7613–7618.

67 Sanchez-Danes A et al. Efficient generation of A9 midbrain dopaminergic neurons by lentiviral delivery of LMX1A in human embryonic stem cells and induced pluripotent cells. Hum Gene Ther 2012;23:56–69.

68 Chung S, Leung A, Han BS et al. Wnt1-lmx1a forms a novel autoregulatory loop and controls midbrain dopaminergic differentiation synergistically with the SHH-FoxA2 pathway. Cell Stem Cell 2009;5:646–658.

69 Castro DS, Hermanson E, Joseph B et al. Induction of cell cycle arrest and morphological differentiation by Nurr1 and retinoids in dopamine MN9D cells. J Biol Chem 2001;276: 43277–43284.

70 Blanchard V, Raisman-Vozari R, Vyas S et al. Differential expression of tyrosine hydroxylase and membrane dopamine transporter genes in subpopulations of dopaminergic neurons of the rat mesencephalon. Brain Res Mol Brain Res 1994;22:29–38.

71 Deister CA, Teagarden MA, Wilson CJ et al. An intrinsic neuronal oscillator underlies dopaminergic neuron bursting. J Neurosci 2009; 29:15888–15897.

72 Grace AA, Bunney BS. The control of firing pattern in nigral dopamine neurons: Single spike firing. J Neurosci 1984;4:2866–2876.

73 Ramayya AG, Zaghloul KA, Weidemann CT et al. Electrophysiological evidence for functionally distinct neuronal populations in the

human substantia nigra. Front Hum Neurosci 2014;8:655.

74 Grace AA, Bunney BS. Intracellular and extracellular electrophysiology of nigral dopaminergic neurons–1. Identification and characterization. Neuroscience 1983;10:301–315.

75 Engel D, Seutin V. High dendritic expression of Ih in the proximity of the axon origin controls the integrative properties of nigral dopamine neurons. J Physiol 2015;593:4905–4922.

76 Grace AA, Bunney BS. The control of firing pattern in nigral dopamine neuons: Burst firing. J Neurosci 1984;4:2877–2890.

77 Celada P, Paladini CA, Tepper JM. GABAergic control of rat substantia nigra dopaminergic neurons: Role of globus pallidus and substantia nigra pars reticulata. Neuroscience 1999;89:813–825.

78 Bayer HM, Lau B, Glimcher PW. Statistics of midbrain dopamine neuron spike trains in the awake primate. J Neurophysiol 2007;98: 1428–1439.

79 Richards CD, Shiroyama T, Kitai ST. Electrophysiological and immunocytochemical characterization of GABA and dopamine neurons in the substantia nigra of the rat. Neuroscience 1997;80:545–557.

80 Lacey MG, Mercuri NB, North RA. Dopamine acts on D2 receptors to increase potassium conductance in neurones of the rat substantia nigra zona compacta. J Physiol 1987; 392:397–416.

81 Thomson JA, Kalishman J, Golos TG et al. Pluripotent cell lines derived from common marmoset (Callithrix jacchus) blastocysts. Biol Reprod 1996;55:254–259.

82 Calhoun JD, Lambert NA, Mitalipova MM et al. Differentiation of rhesus embryonic stem cells to neural progenitors and neurons. Biochem Biophys Res Commun 2003;306:191–197.

83 Sundberg M, Bogetofte H, Lawson T et al. Improved cell therapy protocols for Parkinson's disease based on differentiation efficiency and safety of hESC-, hiPSC-, and non-human primate iPSC-derived dopaminergic neurons. STEM CELLS 2013;31:1548–1562.

84 Ferrari D, Sanchez-Pernaute R, Lee H et al. Transplanted dopamine neurons derived from primate ES cells preferentially innervate DARPP-32 striatal progenitors within the graft. Eur J Neurosci 2006;24:1885–1896.

85 Ikeda R, Kurokawa MS, Chiba S et al. Transplantation of neural cells derived from retinoic acid-treated cynomolgus monkey embryonic stem cells successfully improved motor function of hemiplegic mice with experimental brain injury. Neurobiol Dis 2005;20:38–48.

86 Attanasio R, Jayashankar L, Engleman CN et al. Baboon immunoglobulin constant region heavy chains: Identification of four IGHG genes. Immunogenetics 2002;54:556–561.

87 Scinicariello F, Jayashankar L, Attanasio R. Baboon immunoglobulin variable region heavy chains: Identification of genes homologous to members of the human IGHV1-IGHV7 subgroups. Immunogenetics 2002;53:815–820.

88 Jayashankar L, Brasky KM, Ward JA et al. Lymphocyte modulation in a baboon model of immunosenescence. Clin Diagn Lab Immunol 2003;10:870–875.

89 Rogers KA, Scinicariello F, Attanasio R. IgG Fc receptor III homologues in nonhuman primate species: genetic characterization and ligand interactions. J Immunol 2006;177: 3848–3856.

90 Willis EL, Wolf RF, White GL et al. Age- and gender-associated changes in the concentrations of serum TGF-1β, DHEA-S and IGF-1 in healthy captive baboons (Papio hamadryas anubis). Gen Comp Endocrinol 2014;195:21–27.

91 McFarlane D, Wolf RF, McDaniel KA et al. The effect of season on inflammatory response in captive baboons. J Med Primatol 2012;41: 341–348.

92 Nguyen HN, Byers B, Cord B et al. LRRK2 mutant iPSC-derived DA neurons demonstrate increased susceptibility to oxidative stress. Cell Stem Cell 2011;8:267–280.

93 Devine MJ, Ryten M, Vodicka P et al. Parkinson's disease induced pluripotent stem cells with triplication of the α-synuclein locus. Nat Commun 2011;2:440.

94 Soldner F, Hockemeyer D, Beard C et al. Parkinson's disease patient-derived induced pluripotent stem cells free of viral reprogramming factors. Cell 2009;136:964–977.

95 Kawasaki H, Suemori H, Mizuseki K et al. Generation of dopaminergic neurons and pigmented epithelia from primate ES cells by stromal cell-derived inducing activity. Proc Natl Acad Sci USA 2002;99:1580–1585.

96 Kuo HC, Pau KY, Yeoman RR et al. Differentiation of monkey embryonic stem cells into neural lineages. Biol Reprod 2003;68:1727–1735.

97 Park CH, Minn YK, Lee JY et al. In vitro and in vivo analyses of human embryonic stem cell-derived dopamine neurons. J Neurochem 2005; 92:1265–1276.

98 Cooper O, Hargus G, Deleidi M et al. Differentiation of human ES and Parkinson's disease iPS cells into ventral midbrain dopaminergic neurons requires a high activity form of SHH, FGF8a and specific regionalization by retinoic acid. Mol Cell Neurosci 2010;45:258–266.

99 Han BS, Iacovitti L, Katano T et al. Expression of the LRRK2 gene in the midbrain dopaminergic neurons of the 14 substantia nigra. Neurosci Lett 2008;442:190–194.

100 Ye W, Shimamura K, Rubenstein JLR et al. FGF and Shh signals control dopaminergic and serotonergic cell fate in the anterior neural plate. Cell 1998;93:755–766.

101 Trainor PA, Ariza-McNaughton L, Krumlauf R. Role of the isthmus and FGFs in resolving the paradox of neural crest plasticity and prepatterning. Science 2002;295:1288–1291.

102 Dhara SK, Hasneen K, Machacek DW et al. Human neural progenitor cells derived from embryonic stem cells in feeder-free cultures. Differentiation 2008;76:454–464.

103 Morizane A, Doi D, Kikuchi T et al. Direct comparison of autologous and allogeneic transplantation of iPSC-derived neural cells in the brain of a non-human primate. Stem Cell Rep 2013;1:283–292.

104 Schultz W, Aebischer P. The activity of pars compacta neurons of the monkey substantia nigra in relation to motor activation. Brain Res 1983;51:377–387.

105 Schultz W. Responses of midbrain dopamine neurons to behavioral trigger stimuli in the monkey. J Neurophysiol 1986;56:1439–1461.

106 Gonon FG. Nonlinear relationship between impulse flow and dopamine released by rat midbrain dopaminergic neurons as studied by in vivo electrochemistry. Neuroscience 1988;24:19–28.

107 Cragg SJ, Hille CJ, Greenfield SA. Dopamine release and uptake dynamics within nonhuman primate striatum in vitro. J Neurosci 2000;20:8209–8217.

See www.StemCellsTM.com for supporting information available online.